# RF-based Indoor Moving Direction Estimation using a Single Access Point

Yusen Fan, *Student Member, IEEE*, Feng Zhang, *Member, IEEE*, Chenshu Wu, *Senior Member, IEEE*, Beibei Wang, *Senior Member, IEEE*, and K. J. Ray Liu, *Fellow, IEEE*

***Abstract*—Indoor moving direction and rotation angle measurements are crucial to many ubiquitous mobile computing applications. Most of the state-of-the-art approaches rely on inertial sensors, e.g., accelerometers, gyroscopes and magnetometers, which suffer from severe accumulative errors or accuracy degradation indoors. This paper presents an RF-based direction estimation method, which utilizes the off-the-shelf commodity WiFi devices for accurate moving direction and in-place rotation angle estimation. The proposed approach employs a novel 2D antenna array and leverages the spatial decay property of the time-reversal resonating strength. First, the moving speeds along different directions, specified by the 2D array, are derived using virtual antenna alignment. The precise estimation of the device's moving direction is then achieved by combining the obtained velocity information and the a prior knowledge of the array's geometry layout. Experiments in a multipath-rich indoor environment have shown that the median error for moving direction estimation is 6.9°, which outperforms the accelerometer counterpart. The results also verify the good accuracy of in-place rotation angle estimation without any accumulative error, which beats the gyroscope in long term tests. Because the proposed approach can achieve high accuracy without accumulative drifts, it is a promising candidate solution to applications that require accurate direction information.**

***Index Terms*—Direction finding, time reversal, 2D antenna array, virtual antenna alignment**

## I. Introduction

THE moving direction and rotation angle measurements indoors are crucial to a large variety of applications including indoor positioning and indoor navigation (IPIN) [1]–[4], gesture recognition [5], virtual reality (VR) [6] and so on. For the IPIN alone, the global market is forecast to reach USD 7.8 billion by year 2021 [7], which shows the growing demand and increasing importance in accurate direction measurements.

The mainstream has been resorting to the inertial measurement unit (IMU) [2], [8]–[13], i.e., magnetometer that estimates orientation, gyroscope that calculates angular velocity, and accelerometer that provides linear acceleration, for direction estimation indoors. Those sensors, however, are notorious for their significant errors and drifts that are difficult to recalibrate [14]. Specifically, the magnetometer is severely affected by the ferro-magnetic interference indoors, and it only estimates the device orientation which may not necessarily be the user's heading direction; the gyroscope suffers from considerable accumulative errors introduced by integration, which would be amplified in the long run; the accelerometer measurements are too noisy to infer the moving direction. Such limitations hinder many applications that require accurate direction information, including indoor tracking, gesture control, and VR games.

Wireless sensing is an emerging area that has drawn more and more attention and is promising for various kinds of applications [15], [16]. Particularly, in recent years, much progress has been made for target localization and tracking. Although some novel systems can achieve decimeter level or even centimeter level accuracy in localization [17], [18], they all have the following drawbacks that prohibit ubiquitous precise direction measurements: (1) They cannot directly measure the moving direction but rather can only get a rough estimate from successive location estimates. (2) They are not able to measure the in-place rotation angle. (3) Following triangulation, multiple precisely installed APs and their locations and/or orientations information are needed. (4) They degenerate or even fail in Non-Line-Of-Sight (NLOS) scenarios under rich multipath environments.

In this paper, we propose an RF-based measurement method to estimate the moving direction and in-place rotation angle. It has minimum requirements on the hardware: only a 2D antenna array and an arbitrarily placed AP, without knowing its location or orientation information, are needed. It passively measures the Channel State Information (CSI) at the receiver side from the signals transmitted by the AP. In contrast to IMU-based direction finding methods, which are inaccurate and prone to drifting errors, the proposed method is more precise without accumulative errors. Different from most existing wireless indoor localization and tracking schemes that are flawed or even fail in NLOS, our method works well in strong NLOS scenarios and is resilient to environmental dynamics.

RF-based inertial measurement is recently introduced in [19], [20], which utilizes a technique of virtual antenna alignment (VAA) to infer moving speed, direction, and rotating angle. Albeit high precision has been achieved for moving speed, the resolutions in moving direction and rotating angle are not yet optimized. In this work, we boost the accuracy in moving direction and rotating angle estimation by making use of multiple speed estimates along different aligned antenna pairs. Combining the speed estimates with the known and fixed geometric relations of the antenna array, we propose a novel moving direction estimation algorithm that has continuous resolution with high accuracy. As a simple illustration shown in Fig. 1, the moving direction of the antenna array is close

Y. Fan, F. Zhang, C. Wu, B. Wang, and K. J. R. Liu are with the Department of Electrical and Computer Engineering, University of Maryland, College Park, MD, 20742, and Origin Wireless Inc., Greenbelt, MD, 20770.
E-mail: {ysfan, fzhang15, cswu, bebewang, kjrliu}@umd.edu.

This article has been accepted for publication in a future issue of this journal, but has not been fully edited. Content may change prior to final publication. Citation information: DOI 10.1109/JIOT.2021.3083669, IEEE Internet of Things Journal



to the directions of $\overrightarrow{AB}$ and $\overrightarrow{AC}$ so that antenna pairs $AB$ and $AC$ are roughly aligned, from which the velocities $\overrightarrow{v_1}$ and $\overrightarrow{v_2}$ can be estimated using VAA. The direction of the device's overall velocity $\overrightarrow{v}$ can be derived from the geometric constraints between $\overrightarrow{AB}$ and $\overrightarrow{AC}$.

To ensure the existence of aligned antenna pairs for any heading direction, a novel 2D antenna array is designed. The spatial decay property of the time reversal resonating strength (TRRS), which is first discovered and utilized in indoor localization by [21], is used to guide the design of the 2D antenna array. Based on the spatial decay curve of the TRRS, the antenna pairs that are close to each other before and after the rotation can be inferred from the highest TRRS values. Then, according to the antenna array geometry, the in-place rotation angle can be calculated at a high accuracy without drifting errors.

Experiments in a floor of busy office space, under strong NLOS environment with rich multipaths, verify the accuracy of the proposed algorithms: the median error for moving direction estimation is $6.9^\circ$, which outperforms the accelerometer counterpart. The mean error for rotation angle estimation is $16.6^\circ$, which is comparable with the gyroscope, and much better in the long run without drifting errors. The promising performance and low cost make the proposed direction finding method suitable for applications that need accurate direction information.

In summary, the main contributions of the paper are as follows.

- We propose a novel moving direction estimation algorithm with high-accuracy resolution by utilizing a single AP.
- We design a novel 2D antenna array based on the spatial decay property of the TRRS that enables in-place rotation angle estimation.
- The proposed method has minimum hardware requirement without knowing the location/orientation information of the antenna array and the AP.
- The proposed method outperforms most existing approaches even under NLOS conditions without accumulative errors.

The rest of the paper is organized as follows: In Section II, we discuss the related work. Section III provides the background of TRRS and TR Focusing Ball for the basis of the proposed algorithm. Section IV explains the proposed moving direction and rotation angle estimation algorithm in detail. The experimental evaluation is given in Section V. We discuss the future work in Section VI. Finally, we draw the conclusion in Section VII.

## II. Related Work

The related work can be classified into two categories: IMU-based and RF-based.

### A. IMU-based Direction Finding

The mainstream of indoor direction finding is based on data fusion from IMU sensors. Humaine [12] and SmartPDR [2] use the variation of magnetometer readings, and the correlation between compass and gyroscope measurements to assign different weights on the previous moving direction estimate, magnetometer reading and gyroscope measurement for updating the heading direction. In [22], the authors introduce a complimentary filter to fuse the high-frequency components of the gyroscope and low-frequency components of the magnetometer and accelerometer in the hope of suppressing the drift error of gyroscope. $A^3$ [13] mainly uses gyroscope, and the recalibration is done with the compass and accelerometer. The opportunistic calibration occurs when the changes derived from the compass and gravity are both similar to the gyroscope reading. They all face the problem of unreliable magnetometer readings in the indoor environments, and the calibration opportunities may not be very often.

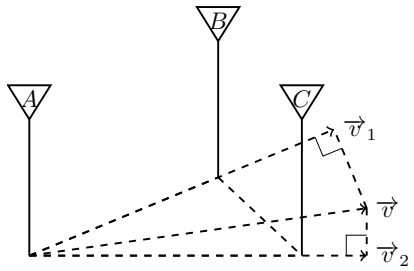


Fig. 1. A simple illustration with three antennas.

Some researchers additionally utilize the periodic patterns of human walking to infer heading direction [9], [10]. [9] identifies the points where acceleration crosses the normal earth gravity value, which indicate that the phone orientation is the same as the original static state. With the assumptions of knowing the initial phone heading offset and stability of the phone's relative orientation with respect to the leg movement, the user's moving direction can be estimated at every step. WalkCompass [10] detects the peaks in the accelerometer readings, and finds the maximum deceleration time point backwards until the time when the acceleration changes from positive to negative. A time window of the corresponding gyroscope readings is extracted and filtered to do dead reckoning of the moving direction. They both utilize the human walking patterns and cannot generalize to the moving direction estimation of robots, drones, and VR devices, etc. What's worse, none of them can solve the side-way movement (change the moving direction without rotating the device).

### B. RF-based Direction Finding

Most of the RF-based methods do not address the direction estimation problem directly. Instead, they focus on solving the localization problem first, and the moving direction can be inferred by successive location estimates. Many explore the geometric channel parameters such as Angle of Arrival (AoA) [17], [18], [23], Time of Flight (ToF) [24], [25], and the fusion of both [26], [27]. Although some can achieve decimeter level accuracy, they require a large phased antenna array or a large frequency bandwidth. To increase the effective bandwidth, frequency hopping technique is used in [28], [29], which, however, introduces the extra spectrum overhead. Moreover,

This article has been accepted for publication in a future issue of this journal, but has not been fully edited. Content may change prior to final publication. Citation information: DOI 10.1109/JIOT.2021.3083669, IEEE Internet of Things Journal



most of them will degrade or even fail under complex NLOS scenarios with rich multipaths because of the principle they are based on: the direct path has to be identified and accurate information about it has to be extracted. On the other hand, fingerprinting-based method has drawn much attention as well [30]–[35]. In [33], the channel impulse response (CIR) is utilized to achieve centimeter level granularity, which is further improved by extending the number of antennas [34] and by frequency hopping technique [35]. Despite of the high accuracy of the fingerprinting-based approaches, they suffer from the environmental dynamics changes. For example, the change of the furnitures may impact the fingerprinting features severely, and the entire database needs to be updated accordingly. In addition, for large areas, not only the constructing of the database is time consuming, but also the computational cost is high for fingerprint matching. These works, again, do not directly obtain direction information.

For the RF-based works that find the direction information directly [19], [36], WiDir [36] estimates the user's walking direction based on the Fresnel zone model. According to the channel frequency response (CFR) power profile affected by a walking person, it makes use of the frequency diversity of OFDM subcarriers to infer the direction in terms of inwards or outwards the Fresnel zone. As the author pointed out, the assumption that distances between adjacent Fresnel contours are the same for different directions, however, is not correct. Also, the subcarrier selection is dependent on the TX and RXs placement, which hinders its ubiquitous deployment. Most importantly, the Fresnel model holds best in LOS scenarios, which cannot work well through multiple walls.

RIM [19] proposes a virtual antenna alignment method, which can estimate the moving distance at a centimeter level accuracy even in NLOS. By implementing a hexagonal antenna array, it can find the best aligned antenna pair, and the moving direction is determined by the two best aligned antennas. What's more, utilizing the estimated moving distance and the radius of the antenna array, it can infer the in-place rotation angle, which cannot be measured by the other RF-based methods. The resolutions of the moving direction and rotation angle estimation, however, are not satisfactory. Our work is inspired by RIM and considerably pushes the accuracy of heading direction and rotation angle.

## III. Preliminaries

In this section, the background of TRRS and TR Focusing Ball is introduced to serve as the basis for the proposed direction estimation algorithm.

### A. Time Reversal Resonating Strength

Time reversal focusing effect is a well known physical phenomenon that the signal's energy is focused (maximized) at a specific time and location instance when combined with its time reversed and conjugated version. Such a spatial-temporal focusing effect is verified on electromagnetic waves by experiment in [37]. Utilizing the focusing effect, [34] can distinguish different locations at a centimeter-level resolution.

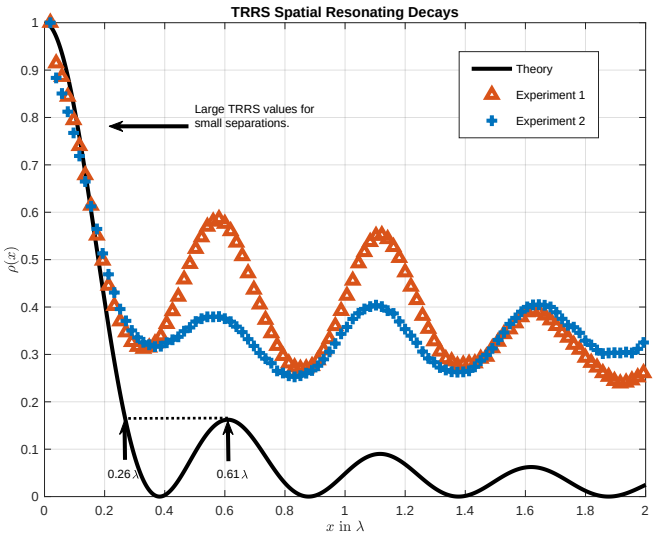


Fig. 2. TRRS spatial decay curve. The solid line shows the Bessel function curve in theory. The dashed lines are from experiments. Note that the peak locations of the experiment agree well with the theory. The separation distance of the first peak is at $0.61\lambda$, and TRRS value is large for small separations.

The concept of TRRS, indicating the similarity level of two CIRs, is first introduced in [33]. We adapt to the equivalent using CFRs: Given two CSIs $H_1$ and $H_2$, the TRRS is defined as:

$$\rho(H_1, H_2) = \frac{|\langle H_1, H_2 \rangle|^2}{|H_1|^2 |H_2|^2}, \tag{1}$$

where $\langle \mathbf{x}, \mathbf{y} \rangle$ denotes the inner product of comlex vectors $\mathbf{x}$ and $\mathbf{y}$, and $|\cdot|$ is the magnitude operator.

Notice that $\rho(H_1, H_2) \in [0, 1]$, and it is equal to 1 if and only if $H_1 = cH_2$, where $c$ is a non-zero complex scaling factor. Thus, TRRS can be indeed used as a similarity metric between CSIs.

### B. Time Reversal Focusing Ball

In the indoor environment, where there exist rich multipath components (MPCs), there exist a critical statistical property for TRRS in spatial domain. For two CSIs $H_1$ and $H_2$ measured at a separating distance $x$, their TRRS can be approximated as a determinate function [21]:

$$\rho(H_1, H_2) \approx J_0^2(\frac{2\pi}{\lambda} x), \tag{2}$$

where $J_0(x)$ is the zeroth-order Bessel function of the first kind, and $\lambda$ is the wavelength. The theoretical and measured TRRS spatial decay curves are shown in Fig. 2.

It has to be pointed out that due to the asymmetric normalized energy distribution of MPCs in certain directions, the actual TRRS is a superposition of $J_0^2(\frac{2\pi}{\lambda} x)$ and some unknown function. Nevertheless, the damping pattern (locations of local minima and local maxima) agrees well with the theoretical Bessel function result. Hence, the moving speed can be calculated from dividing the identified first peak position by the corresponding time lag as in [21].

This article has been accepted for publication in a future issue of this journal, but has not been fully edited. Content may change prior to final publication. Citation information: DOI 10.1109/JIOT.2021.3083669, IEEE Internet of Things Journal



## IV. Proposed Algorithm

Based on the TRRS spatial decay curve, a novel algorithm for estimating the moving direction and the rotation angle is proposed in this section.

### A. Overview

A two dimensional circular antenna array, where one additional antenna is at the center, and the reference coordinate system are shown in Fig. 3. Denote the number of antennas on the periphery as $n_{per}$, then the circumferential angle between adjacent peripheral antennas is $\alpha = 180°/n_{per}$.

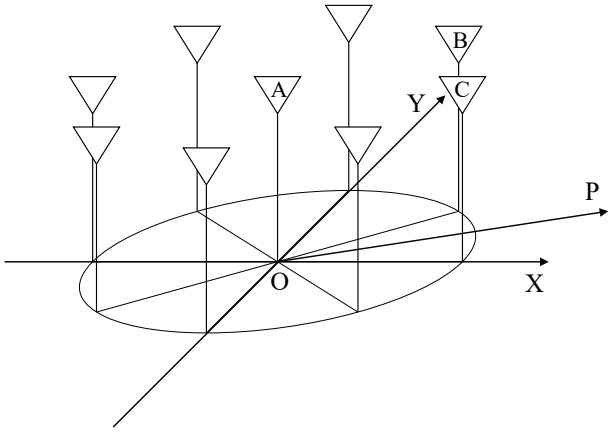


Fig. 3. Designed octagon antenna array for direction measurement.

For the moving direction estimation, denote the moving direction as $\overrightarrow{OP}$. There are several pairs of antennas whose traces are close to each other, which are denoted as aligned antenna pairs, and we take 3 antennas $A, B, C$ for illustration.

Denote the CSIs measured by those antennas at time $t$ as $H_A(t), H_B(t)$ and $H_C(t)$. For the CSIs collected at the same time, the corresponding separations between antenna $AB$, and antenna $AC$ are both the radius, which is chosen as half the wavelength. From the TRRS spatial decay curve in Fig. 2, the TRRS values $\rho(H_A(t), H_B(t))$ and $\rho(H_A(t), H_C(t))$ are small. Imagine antenna $A$ keeps moving and collecting CSIs along the heading direction $\overrightarrow{OP}$. At time $t+\delta_{AB}$, the antenna $A$ is closest to the location of antenna $B$ at time $t$, thus $\rho(H_A(t + \delta_{AB}, H_B(t))$ yields a large value. Similarly, we expect to observe a large value for $\rho(H_A(t + \delta_{AC}, H_C(t))$. From the large TRRS values, we can infer that the moving direction is close to the directions indicated by $\overrightarrow{AB}$ and $\overrightarrow{AC}$. Hence, by identifying antenna pairs with high TRRS values, the rough heading direction is determined by the selected antenna pairs. The details are revealed in the later sections for finding the correct antenna pairs.

Furthermore, utilizing the time antenna $A$ takes to reach the closest locations to antenna $B$ and antenna $C$, namely $\delta_{AB}$ and $\delta_{AC}$, we can refine the direction estimation together with the geometry of the 2D antenna array, which will be explained in the following sections.

For the in-place rotation angle estimation, assume the antenna array rotates about $\alpha$ clockwise. There are several pairs of antennas whose ending locations are close to the starting locations. Taking antennas $B$ and $C$ as an example, the ending location of antenna $B$ is close to the starting location of antenna $C$, thus the TRRS between them should yield a large value. For different rotation angles, the pairs of antennas with high TRRS values will vary accordingly. By calculating the TRRS values between the CSIs collected at the beginning and after rotating, the rotation angle can be estimated using the high TRRS values and the geometric relations of the antenna array.

### B. Nearest Location Identification

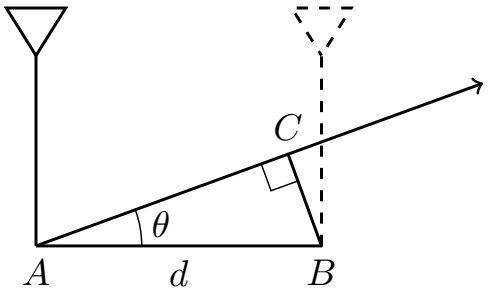


Fig. 4. Nearest location identification using CSI. The solid antenna is moving from A to C and captures the CSIs along the trace. The CSI at location B is measured and known. It is expected to have highest TRRS value between CSI at location C and that at location B under certain geometric restrictions.

In this section, we explore the geometric constraint on the correctness of mapping from the largest TRRS value to the closest physical location from one moving antenna to the other anchor antenna, which guides our design of the 2D antenna array in the next section.

As illustrated in Fig. 4, the moving antenna, of which the initial location is $A$, moves along the trace $\overrightarrow{AC}$. The reference location is $B$, whose CSI $H_B$ is measured by another antenna in advance. The distance between $A$ and $B$ is $d$, and the angle $\angle BAC$ is $\theta$. Let $H_A(t)$ denote the CSIs measured by the moving antenna, and time $t = 0$ be the moment it starts moving.

From a geometric point of view, the nearest point on the moving trace to the reference location is the projection of $B$ onto the moving trace, namely the point $C$. To identify this closest location using CSI measurements, the hope is that CSIs at closest locations exhibit highest level of similarity, i.e., largest TRRS. If this is the case, the CSI at point $C$, $H_C$, can be directly inferred from the largest TRRS:

$$H_C = \underset{H_A(t)}{\arg\max}\, \rho(H_A(t), H_B), \tag{3}$$

and the time instance at the nearest location can be extracted from $H_C$ accordingly.

From the theoretical TRRS spatial decay curve, however, the nearest geometric location does not always imply highest level of similarity in CSIs. To make such an implication holds, there is a constraint on the initial distance $d$ and the angle $\theta$. The principle is that the TRRS at the nearest location should be higher than that of the first peak at $0.61\lambda$ to avoid ambiguity, as

shown in Fig. 2,which means, equivalently, the closest distance must be less than $0.26\lambda$:

$$d\sin(\theta) < 0.26\lambda \tag{4}$$

For $d = \lambda/2$, $\theta$ should be less than $31°$. Eqn. (4) serves as a guidance on designing the two-dimensional antenna array in the following section.

### C. Aligned Antenna Pairs Selection

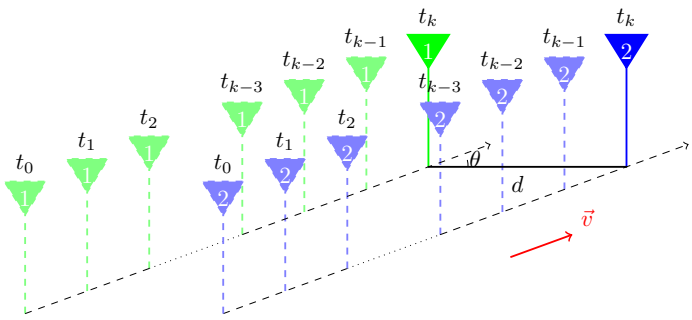


Fig. 5. The two-antenna linear array moving trace. For a small deviation angle $\theta$, the largest TRRS between CSIs of two antennas should map to the closest geometric location, which can be used to calculate the moving speed in terms of $\theta$.

In this section, we explain the reasons for the design of the 2D antenna array, and introduce the method of finding best aligned antenna pairs of the 2D array to indicate the rough estimate of the moving direction, which provides a starting point for the algorithm in Section IV-D.

Before introducing the two-dimensional antenna array, a linear array composed of two antennas with a separating distance $d$ is studied first. Assume the array is moving with a deviation angle $\theta$ relative to its orientation, as shown in Fig. 5. Let the CSIs of the two antennas measured along the way be $H_1(t_i)$ and $H_2(t_i)$, where $i = 0, 1, 2, ..., k$ represents the sampling index. From the previous discussion, if the deviation angle $\theta$ is small enough, the largest TRRS should map to the nearest location to a reference point. In other words, given the reference location as the position of antenna 2 at time $t_i$, the time delay antenna 1 takes from time $t_i$ to the closest location can be calculated as:

$$\Delta t = \arg\max_{\Delta t} \rho(H_1(t_i + \Delta t), H_2(t_i)), \tag{5}$$

where $\Delta t$ can be a negative value if antenna 2 is moving towards antenna 1.

If the antenna separation $d$ and deviation angle $\theta$ are known, the moving distance $l$ can be derived from the geometric relation: $l = d\cos(\theta)$, as illustrated in Fig. 4. Making use of the corresponding time delay $\Delta t$, the velocity $v$ is further obtained by:

$$v = \frac{d\cos(\theta)}{\Delta t}, \tag{6}$$

which is important for the direction estimation in the next section.

To find out the time delay $\Delta t$, a TRRS vector $\mathbf{g}(t_i)$ is calculated through a window of length $2W + 1$ centered at $t_i$:

$$\mathbf{g}(t_i) = [\rho(H_1(t_{i+j}), H_2(t_i)), j = -W, ..., W]^T, \tag{7}$$

where $T$ denotes the transpose operator. The window length is decided by the antenna separation, moving speed and the sampling rate. If the speed is too slow, the peak index would lie out of the $W = 50$ window length; if the speed is too fast, the peak index would be 0. In general,

$$\frac{1}{f_s} < \frac{d}{v} < \frac{W}{f_s}, \tag{8}$$

where $d$ denotes the antenna separation and $f_s$ represents the sampling rate.

To find out the time delay at every time index, a TRRS matrix $G$ is formed by concatenating the TRRS vectors:

$$G = [\mathbf{g}(t_1), \mathbf{g}(t_2), ..., \mathbf{g}(t_T)]. \tag{9}$$

Then, the time delay vector $\mathbf{d}(G)$ can be calculated as:

$$\mathbf{d}(G) = [\arg\max \mathbf{g}(t_i) - W, i = 1, 2, ..., T]^T, \tag{10}$$

and the $i^{th}$ element $d(G, i)$ is the time lag at time $t_i$.

Fig. 6 shows the TRRS matrices for deviation angles $0°$, $10°$, $20°$ and $30°$, of which the data is collected using two antennas $\frac{\lambda}{2}$ away from each other. From Eqn. (4), the deviation angle should be less than $31°$ to yield a maximum TRRS at the nearest location, which means a peak at each column of the TRRS matrices. Clear peak traces across time exist for deviation angles $0°$, $10°$ and $20°$. For $30°$, however, the peak trace is hard to find because of the asymmetric energy distribution of MPCs and noise.

Based on both the theoretical and experimental results, a two-dimensional antenna array is designed for the purpose of high accuracy, super resolution moving direction and rotation angle estimation. The designed antenna array is shown in Fig. 3, where eight antennas are uniformly placed on a circle with a radius of half the wavelength, and one antenna is placed at the center. Again, we denote the circumferential angle between adjacent peripheral antennas as $\alpha = 22.5°$. The reasons behind the design are:

1) To measure the moving direction and the rotation angle in $[0°, 360°)$, a circular array is chosen because of the symmetric geometry.

2) For the purpose of high resolution, an octagon array is used based on the peak traces result of TRRS matrices demonstrated in Fig. 6. Consider the directions formed by all the antenna pairs in the array, which are from $0°$ to $360°$ with an increment of $\alpha = 22.5°$. As Fig. 6 shows, clear peak traces can be observed in the TRRS matrices with a deviation around $20°$. Thus, for any arbitrary moving direction, the best aligned antenna pair can be identified, yielding a high resolution of $\alpha = 22.5°$.

3) For the purpose of super resolution and high accuracy, one additional antenna is introduced to leverage the geometric relations of the array. By placing one antenna at the center, it is guaranteed to have at least two aligned pairs of antennas, forming different directions, for any moving direction. Thus,

the continuous resolution of moving direction can be achieved by utilizing the speed estimates and geometry of the aligned pairs, which will be explained further in the next section.

The aligned antenna pairs are those whose orientations are close to the moving direction. By correctly detecting best aligned antenna pairs, the moving direction can be inferred in the vicinity of the directions formed by best aligned antennas. The TRRS matrix is utilized for this purpose: the clearer the peak trace is, the better the alignment of antennas will be. To determine clear peak traces, a peak trace score of a TRRS matrix $G$ is defined as:

$$s(G) = e(G) - \eta\sigma(G), \tag{11}$$

where $e(G)$ is the averaged energy of the peak trace:

$$e(G) = \frac{1}{T}\sum_{i=1}^{T}\max(\mathbf{g}(t_i)), \tag{12}$$

and $\sigma(G)$ is the standard deviation of the time lags in the peak trace:

$$\sigma(G) = \sqrt{\frac{\sum_{i=1}^{T}(d(G,i) - \overline{\mathbf{d}}(G))^2}{T-1}}, \tag{13}$$

where $\overline{\mathbf{d}}(G)$ is the mean of the time delay vector:

$$\overline{\mathbf{d}}(G) = \frac{1}{T}\sum_{i=1}^{T} d(G,i), \tag{14}$$

with $\eta > 0$ as a scaling factor weighting the importance between the energy and coherence of a peak trace.

The best aligned antenna pairs are selected with highest scores. Denote $a(G)$ as the direction corresponding to the TRRS matrix $G$. Note that different antenna pairs may have the same orientation and form the same direction (e.g., the antenna pairs that are parallel to each other), thus we further define the score of a given direction $\phi$ as the maximum one:

$$s(\phi) = \max_{a(G)=\phi} s(G). \tag{15}$$

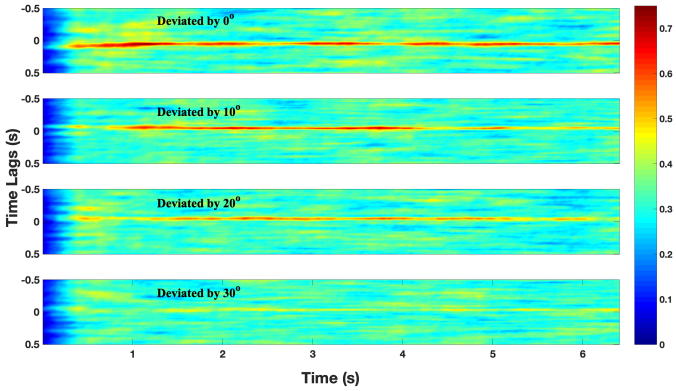


Fig. 6. TRRS matrices for different deviation angles. Clear peak traces (dark traces along time) can be identified except the bottom one.

### D. Moving Direction Estimation

Estimating the moving direction consists of two steps: determining a rough angle range based on best aligned antenna pairs, and estimating the direction within the range using geometric relations to achieve super resolution and high accuracy.

Fig. 7a illustrates the angle range estimation. Assume that $\overrightarrow{OY}$ represents the direction $\theta$ formed by the best aligned antenna pair, i.e., the antenna pair with highest score of their TRRS matrix: $\theta = \arg\max_\phi s(\phi)$. From Fig. 6, the highest TRRS value represents the smallest deviation angle, as depicted in Fig. 5, between the true moving direction and the direction formed by the antenna pair. Hence the true moving direction should be close to this direction formed by the best aligned antenna pair. Three candidate regions are divided: $[\theta-\alpha, \theta]$, $[\theta-\frac{2}{3}\alpha, \theta+\frac{2}{3}\alpha]$ and $[\theta, \theta+\alpha]$, as shown in the figure. Our intuition is that if the score of the direction $\overrightarrow{OX}$, $s(\theta-\alpha)$, is much higher than that of the direction $\overrightarrow{OZ}$, $s(\theta+\alpha)$, the true moving direction should be closer to $\overrightarrow{OX}$, and vice versa. For the case where $s(\theta-\alpha)$ is similar to $s(\theta+\alpha)$, the true direction is likely to lie in the middle. Translating the intuition into implementation, the following ratios are calculated:

$$\begin{aligned}\beta_1 &= \frac{\frac{s(\theta)+s(\theta-\alpha)}{2} - s(\theta+\alpha)}{s(\theta) - s(\theta-\alpha)}\\ \beta_2 &= \frac{\frac{s(\theta)+s(\theta+\alpha)}{2} - s(\theta-\alpha)}{s(\theta) - s(\theta+\alpha)}.\end{aligned} \tag{16}$$

Then, they are compared with a positive threshold $\beta$, respectively. If $\beta_1 > \beta$, $s(\theta+\alpha)$ is too small to be chosen, and the estimated range is Region 1. Similarly, if $\beta_2 > \beta$, Region 3 is selected as the angle range. If neither of the conditions holds, the true moving direction most likely resides in Region 2.

After the rough range estimation, a finer direction estimation can be achieved utilizing the geometric relations and time delays of peak traces in the selected TRRS matrices. There are two cases: (1) Only two different (adjacent) directions have clear peak traces (high scores) in the corresponding TRRS matrices, referring to Region 1 and 3 in Fig. 7a. (2) Three different (adjacent) directions with clear peak traces in the TRRS matrices can be found, as the Region 2 in Fig. 7a.

For the first case, let antenna pairs $AB$ and $CD$ be the best aligned pairs for the two adjacent directions, as shown in Fig. 7b. Denote the distance between $AB$ as $d_1$ and the distance between $CD$ as $d_2$. The moving direction is the direction pointed by the arrow, which lies in the $\alpha$ angle range. The deviation of the moving direction from $\overrightarrow{CD}$ is $\gamma$, thus the angle between the moving direction and $\overrightarrow{AB}$ is $\alpha-\gamma$. Referring to Eqn. (6), the velocities calculated using $AB$ and $CD$ are:

$$\begin{aligned}v_1 &= \frac{d_1\cos(\alpha-\gamma)}{\Delta t_1}\\ v_2 &= \frac{d_2\cos(\gamma)}{\Delta t_2},\end{aligned} \tag{17}$$

where $\Delta t_1$ and $\Delta t_2$ are the time delays of peak traces in the TRRS matrices of $AB$ and $CD$, respectively. Since the size of the antenna array is small, at the scale of wavelength (5.17cm

This article has been accepted for publication in a future issue of this journal, but has not been fully edited. Content may change prior to final publication. Citation information: DOI 10.1109/JIOT.2021.3083669, IEEE Internet of Things Journal



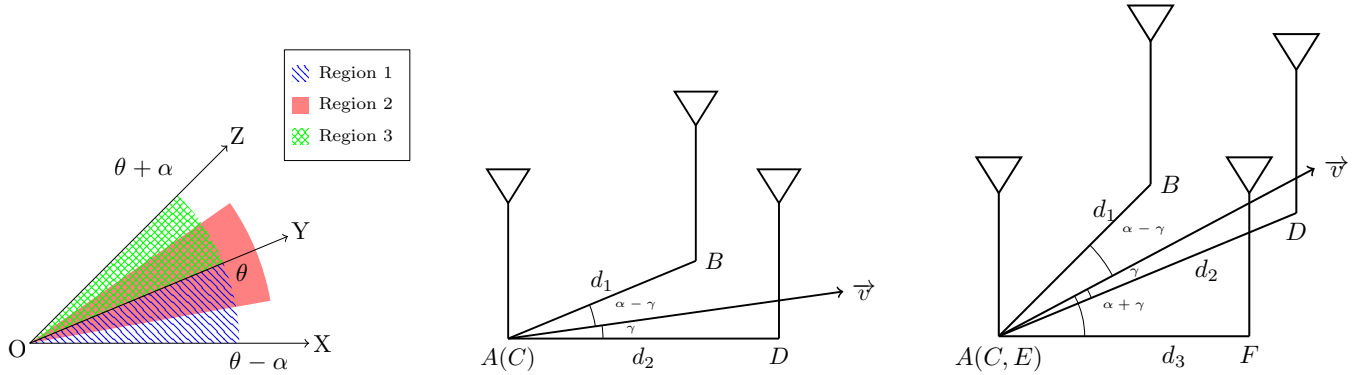


(a) Angle regions illustration.

(b) Case 1: the moving direction is either in Region 1 or Region 3.

(c) Case 2: the moving direction is in Region 2.

Fig. 7. Angle range estimation

for $f_0 = 5.8$GHz), the moving speed cannot vary much in such a short distance:

$$\begin{aligned} v_1 &\approx v_2 \\ \frac{d_1\cos(\alpha-\gamma)}{\Delta t_1} &\approx \frac{d_2\cos(\gamma)}{\Delta t_2} \\ \gamma &\approx tan^{-1}(\frac{\frac{d_2\Delta t_1}{d1\Delta t_2}-\cos\alpha}{\sin\alpha}). \end{aligned} \tag{18}$$

Then, the estimate of $\gamma$ is calculated as:

$$\hat{\gamma} = tan^{-1}(\frac{\frac{d_2\Delta t_1}{d1\Delta t_2}-\cos\alpha}{\sin\alpha}). \tag{19}$$

For the second case, the geometric relations are demonstrated in Fig. 7c, with the meaning explained in Fig. 7b. Similar to the first case, the velocities can be estimated using each pair of antennas:

$$\begin{aligned} v_1 &= \frac{d_1\cos(\alpha-\gamma)}{\Delta t_1} \\ v_2 &= \frac{d_2\cos(\gamma)}{\Delta t_2} \\ v_3 &= \frac{d_3\cos(\alpha+\gamma)}{\Delta t_3}. \end{aligned} \tag{20}$$

The estimated $\gamma$ is calculated as:

$$\hat{\gamma} = \arg\min_{\gamma} \quad (v_1-v_2)^2+(v_3-v_2)^2, \tag{21}$$

where $\hat{\gamma}$ can be derived as:

$$\hat{\gamma} = \tan^{-1}(\frac{\frac{d_2\Delta t_3}{d_3\Delta t_2}-\frac{d_2\Delta t_1}{d_1\Delta t_2}}{2\sin\alpha}). \tag{22}$$

Summarizing the above discussion in this section, the detailed moving direction estimation algorithm is described in Algorithm 1.

**Algorithm 1** Moving Direction Estimation

**Input:**
$\{G\}$ : set of TRRS matrices for all pairs of antennas;
$a(G)$: direction of the antenna pair with TRRS matrix $G$;
$\eta$ : positive scaling factor;
$\beta$ : positive threshold
**Output:**
$\theta$: estimated moving direction
**Procedure:**

**for** $G \in \{G\}$ **do** ▷ *initialization*
  $\phi = a(G)$
  $s(\phi) = -\infty$
$s_{max} = -\infty$
**for** $G \in \{G\}$ **do** ▷ *calculating scores on each direction*
  $s(G) = e(G) - \eta\sigma(G)$
  $\phi = a(G)$
  **if** $s(G) > s(\phi)$ **then**
    $s(\phi) = s(G)$
    $a(\phi) = a(G)$
$\theta = a(\arg\max_G s(G))$
*calculate ratios* $\beta_1$ *and* $\beta_2$ ▷ *angle range estimation*
**if** $\beta_1 > \beta$ **then** ▷ $[\theta-\alpha, \theta]$
  *calculate* $\hat{\gamma}$ *according to Eqn. (19)*
  **return** $\theta - \alpha + \hat{\gamma}$
**else if** $\beta_2 > \beta$ **then** ▷ $[\theta, \theta+\alpha]$
  *calculate* $\hat{\gamma}$ *according to Eqn. (19)*
  **return** $\theta + \hat{\gamma}$
**else** ▷ $[\theta - \frac{2}{3}\alpha, \theta + \frac{2}{3}\alpha]$
  *calculate* $\hat{\gamma}$ *according to Eqn. (22)*
  **return** $\theta + \hat{\gamma}$

### *E. In-Place Rotation Estimation*

Similar to the moving direction, the TRRS value is also used for determining the in-place rotation angle. The rationale behind the algorithm is that if antenna $i$ on the periphery rotates to a position closest to the starting location of antenna $j$ on the periphery, as shown in Fig. 8, it is expected that the TRRS between those two CSI measurements ($i_{end}$, $j_{start}$) yields a high value, which can be used to infer the rotation angle.

More precisely, let $H_j(t_1)$ denote the CSI measurement of antenna $j$ at time $t_1$, and $H_i(t_2)$ be the CSI measured by antenna $i$ at time $t_2$, where both the antenna $i$ and $j$ are on the periphery. To estimate the rotation angle from $t_1$ to $t_2$, we have to correctly identify the aligned pairs of antennas between $t_1$ and $t_2$. The TRRS values between all pairs of antennas on the periphery are calculated as in Eqn. (23):

$$\rho_{ij} = \rho(H_i(t_2), H_j(t_1)). \tag{23}$$

This article has been accepted for publication in a future issue of this journal, but has not been fully edited. Content may change prior to final publication. Citation information: DOI 10.1109/JIOT.2021.3083669, IEEE Internet of Things Journal



Denote the rotation angle from antenna $i$ to antenna $j$ as $a_{ij}$. Notice that for different pairs of antennas, they may have the same rotation angle. For example, the rotation angle is $2\alpha$ for all the adjacent antenna pairs. Thus, the TRRS values for antenna pairs with same rotation angle can be averaged to suppress noise as follows:

$$\rho_a = \frac{1}{n} \sum_{a_{ij}=a} \rho(H_i(t_2), H_j(t_1)), \tag{24}$$

where $\rho_a$ denotes the averaged TRRS value for rotation angle $a$, and $n$ represents the number of antenna pairs with a rotation angle of $a$.

Following Eqn. (24), the rotation angle is estimated as the one with maximum TRRS value:

$$\hat{a} = \arg\max_a \rho_a. \tag{25}$$

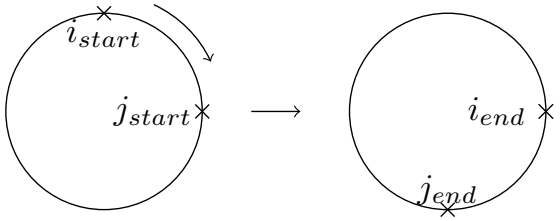


Fig. 8. In-place rotation aligned pairs. The antenna i rotates to a location closest to the initial position of antenna j.

## V. Experiment Results

In this section, we show the experiment results to verify the performance of the proposed algorithm on both the moving direction and rotation angle estimation. We do not compare with AoA based methods because of the drawbacks of the existing approaches utilizing wireless signals mentioned in Section I. Instead, we compare with IMU-based approached in the experiment.

### A. Experiment Design

*1) Hardware Platform:* We use the commercial WiFi NICs, Qualcomm Atheros 9k chipsets, to build the system. For the comparison with IMU sensors, the chipset is attached to an Intel Galileo Gen2 microcontroller board equipped with a Bosch Sensortec BNO055 sensor unit. For the 2D octagonal antenna array composed of 9 antennas, because of the lack of chipsets and microcontrollers, we use 6 antennas of two WiFi NICs to form a half octagonal array as shown in Fig. 9. Although the performance will degrade from 9 antennas to 6 antennas, the half octagonal antenna array can still validate the proposed algorithm as the experiment results shown in the next section.

*2) Software Implementation:* For collecting CSI on Galileo Gen2 board, a tool written in C++ is developed. Then the core functions are implemented using Matlab to evaluate the system performance.

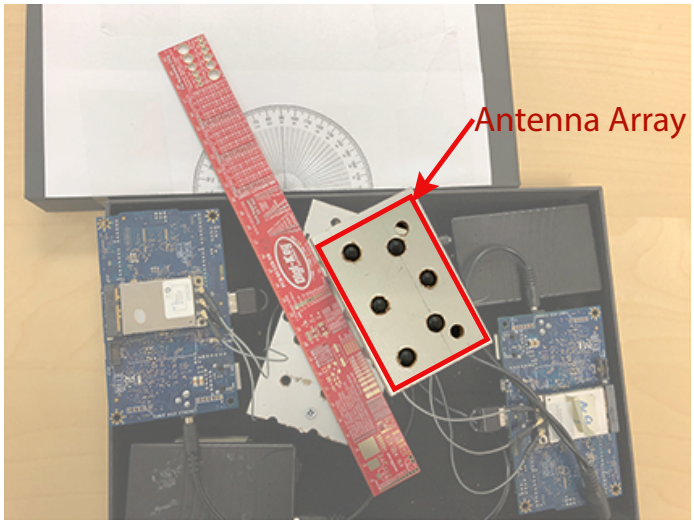


Fig. 9. Experimental Prototype with a Two Dimensional Antenna Array

*3) Ground Truth:* For getting the ground truth of moving direction, a printed protractor and a ruler are used to adjust the orientation of the antenna array with respect to the rectangle box that contains the array. Then, the antenna array is fixed to the rectangle box, and the rectangle box is pushed along a straight track confined by two fixed parallel wooden boundaries. To acquire the ground truth for rotation angle, a rotating plate is used and aligned with the center of the printed protractor. The center of the half octagonal array is also aligned with the protractor center.

*4) Comparison Baselines:* We compare the performance of the proposed algorithm with IMU sensors. Specifically, for the moving direction estimation, the accelerometer is used for comparison. For the rotation angle estimation, the gyroscope is utilized for comparison.

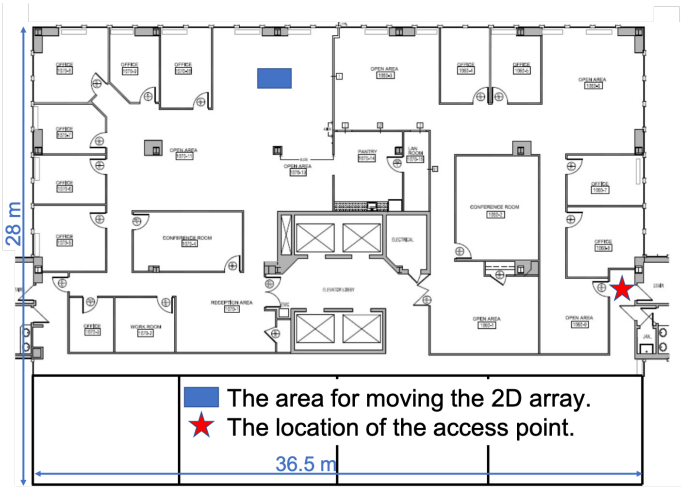


Fig. 10. Experiment Environment. The experiment is conducted in a busy office floor, with furnitures, computers and walking people. The antenna array is far away from the AP and works in a strong NLOS scenario.

*5) Experiment Environment:* The experiments are conducted in an indoor office environment, as shown in Fig. 10. The space is filled with furnitures including desks, chairs and

computers, which are not shown for brevity. The positions of the single AP and the antenna array moving area are labeled accordingly, between which the distance is larger than 25m, and it is a strong NLOS scenario. During the experiments, the AP broadcasts packets continuously at the rate of 200 Hz, on the 5 GHz frequency band with a bandwidth of 40 MHz.

### B. Experiment Results

Now, we show the results from the experiment.

*1) Moving Direction Estimation:* The accuracy of moving direction estimation is compared with the accelerometer since it is the only IMU sensor that can sense the moving direction with respect to the local coordinate. The magnetometer reading shows the orientation of the device, which is not necessarily the same as the moving direction.

We move the 2D antenna array in various directions, ranging from $0^\circ$ to $90^\circ$ with an increment of $10^\circ$. For each direction, the device is moved for about 1 meter.

To estimate the moving direction using the accelerometer, before moving the antenna array, the first step is to do the calibration to remove the offset. The device is first placed on a desk statically, and the readings are averaged as an estimation of the offset to be subtracted. After collecting the accelerometer readings during moving, the offset estimation is subtracted from them. Next, a moving average is used as a low pass filter to filter the calibrated data. Based on the filtered data, the velocity estimation is derived by integrating the acceleration. Finally, the moving direction in the $2D$ plane is calculated using the velocities in the $X$ and $Y$ axes.

As shown in Fig. 11a, the overall median error of the proposed method is $6.9^\circ$, and the 90 percentile error is $19.5^\circ$, which are both better than the accelerometer counterpart: $8.3^\circ$ and $34.9^\circ$. For different moving directions, the proposed method shows a consistent good performance of less than $10^\circ$ median error for all the moving directions as depicted in Fig. 11b, although some directions are slightly worse because of the asymmetry of the half octagonal array.

*2) Rotation Angle Estimation:* To evaluate the performance of the rotation angle estimation, the antenna array is attached on a rotating plate and rotated by various angles of $45^\circ, 90^\circ, 135^\circ, 180^\circ, 360^\circ, 720^\circ, 1080^\circ$. Each angle is repeated by 20 times and the corresponding error is recorded. As depicted in Fig. 12b, the closest rotation angle is correctly identified for most of the cases, except for $135^\circ$ and $180^\circ$. The reason for the worse performance of these two rotation angles is the asymmetry of the half octagonal array. There are few antenna pairs aligning with each other for these two angles. Thus the TRRS calculation is subject to noise and not as robust as other angles. Nevertheless, as shown in Fig. 12a, the mean error is only $16.615^\circ$, which is still comparable to the gyroscope ($16.623^\circ$). More importantly, the proposed method does not have accumulative errors, but the error for gyroscope keeps increasing as the rotation angle increases shown in Fig. 12b. Hence, the proposed algorithm is better than the gyroscope especially for large rotating angles.

*3) Impact of Sampling Rate:* The impact of sampling rate on the moving direction estimation is studied. We downsample the CSI from 200 Hz to 20, 40, 60, 100 and 160 Hz, respectively. The integrated result is shown in Fig. 13. There is a general trend, as expected, that the accuracy increases with higher sampling rates. As pointed out in Eqn. (8), however, higher sampling rate requires larger window length $W$, which increases the computational overhead. Generally, for a fixed antenna array, the required sampling rate for moving direction estimation is determined by the moving speed. For the rotation angle estimation, since only the CSIs at the starting location and ending location are needed, sampling rate is not important.

*4) Accumulative Error on Moving Direction:* To validate that the proposed algorithm is free of accumulative error on moving direction estimation, experiments are done for heading directions of $0^\circ$, $22.5^\circ$ and $45^\circ$ over long moving distances (around 13 m). The precise mapping from time stamps to moving distances is not obtained, but rather the rough distance estimation is derived by assuming a constant 1 m/s moving speed. As can be seen in Fig. 14, there is no accumulative error for the proposed method utilizing the antenna array. For the accelerometer, however, because the velocity is integrated by acceleration over time, a drifting error is thus introduced.

*5) Resilience to dynamic environments:* In this section, we demonstrate the robustness of the proposed method to motion in the environment. There are always two people performing the experiments around the receiving antenna array, in addition to others working normally in the business building. When an experimenter moves the antenna array (either pushing it for heading direction experiment or rotating it for rotation angle experiment), his/her body is moving closely to the receiver, changing the multipath distributions. The experimental results shown above have verified the robustness to the environmental dynamics like these. There are two main reasons behind: 1) There are a large number of multipaths indoors coming from various directions. The human motion will only change part of them, and the TRRS behavior as shown in Fig. 6 still holds. 2) We do not rely on absolute TRRS values, which may change with environmental dynamics.

## VI. Discussion and Future Work

In this section, we discuss the potential improvements on the proposed direction finding system.

### A. Rotation Angle Resolution

Although the accuracy of the in-place rotation angle estimation is comparable to the gyroscope, the resolution is currently discrete, which is determined by the number of antennas in the array. One obvious way to improve the resolution is to increase the number of antennas, but the drawbacks are the complexities on both the hardware and software, and also the increasing size of the array. It remains open to achieving continuous resolution on rotation angle estimation using RF signals.

### B. Antenna Number and Array Size

The proposed system seems to require a large number of antennas, but it is necessary to have the proposed number

This article has been accepted for publication in a future issue of this journal, but has not been fully edited. Content may change prior to final publication. Citation information: DOI 10.1109/JIOT.2021.3083669, IEEE Internet of Things Journal



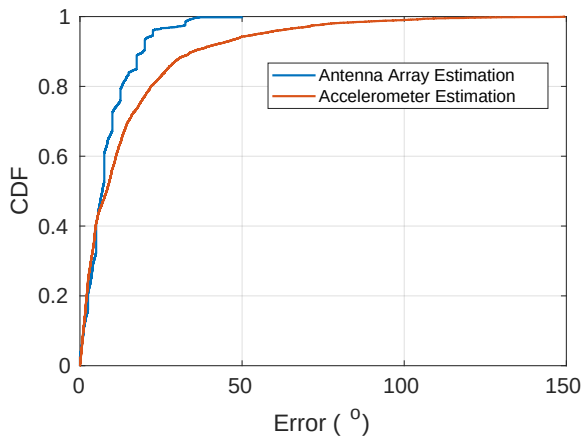


(a) Error CDF for moving direction estimation

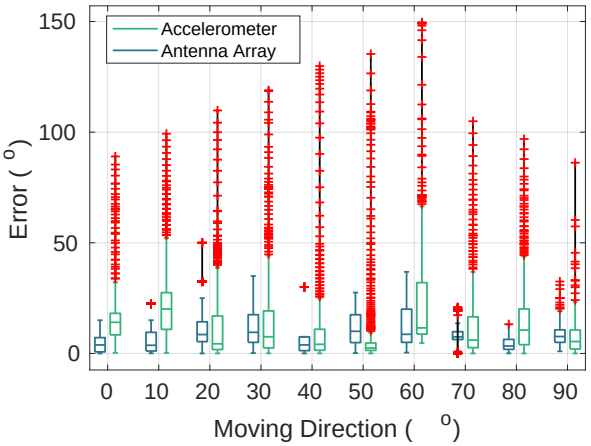


(b) Error bar for different moving directions

Fig. 11. Accuracy on moving direction estimation.

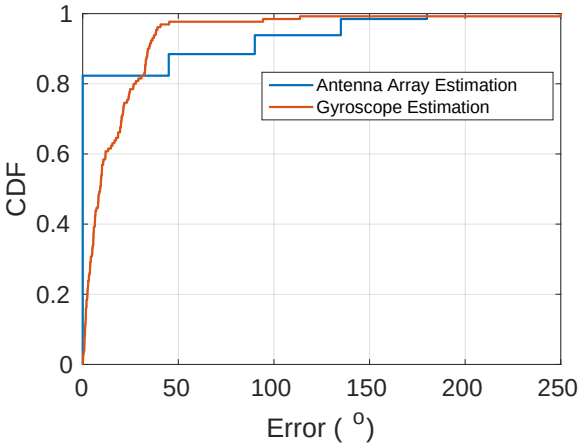


(a) Error CDF for rotation angle estimation

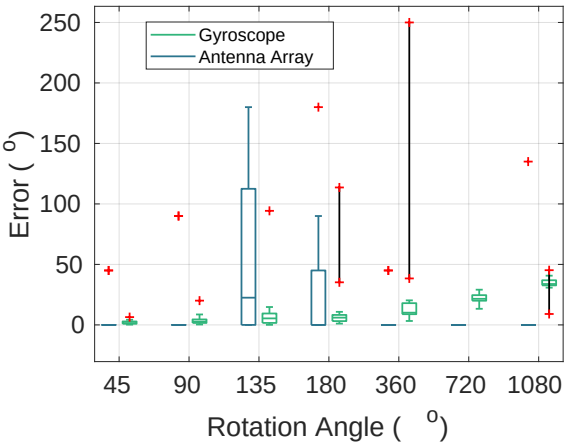


(b) Error bar for different rotation angles

Fig. 12. Accuracy on rotation angle estimation.

of antennas for high accuracy as explained in Section IV-C. Because of the number of antennas, the current size of the antenna array seems large, especially compared to the mobile phones, but it is already attractive for dedicated industrial applications such as robots and tracking carts. With the maturing of WiFi technology with many antennas on a chip and at higher carrier frequencies, e.g., 60 GHz, the size will be small enough to be embedded in mobile devices. We look forward to next-generation MIMO radios that will have large antenna arrays. In the meantime, we will investigate how to reduce the number of required antennas while maintaining similar accuracy.

### C. Direction Finding in 3D

While the proposed system estimates directions accurately in 2D, it cannot measure the 3D directions. One possible approach is to build a dedicated 3D antenna array to find aligned pairs in 3D, which is useful particularly for drones. Again, with the development of 5G technology, the short wavelength of the millimeter wave will make the design of a 3D antenna array more feasible.

## VII. Conclusion

In this paper, we present an RF-based direction estimation method that can accurately measure the moving direction and in-place rotation angle indoors using commercial WiFi radios. The proposed algorithm works well in strong NLOS scenarios over a large dynamically changing environment, which is covered by a single arbitrarily placed AP with unknown location. Because of the low cost on the minimum requirement of hardware, and the high accuracy of $6.9^\circ$ median error for moving direction and $16.6^\circ$ mean error for rotation angle, without drifting errors, it provides a promising solution to a large variety of new applications that require accurate direction information, such as robot tracking, VR gaming and gesture control.

## References

[1] C. Wu, F. Zhang, B. Wang, and K. J. R. Liu, "Easitrack: Decimeter-level indoor tracking with graph-based particle filtering," *IEEE Internet of Things Journal*, vol. 7, no. 3, pp. 2397–2411, 2020.

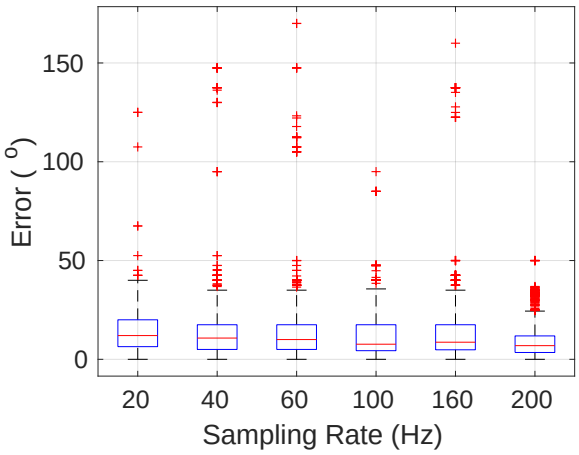


Fig. 13. Sampling Rate Impact

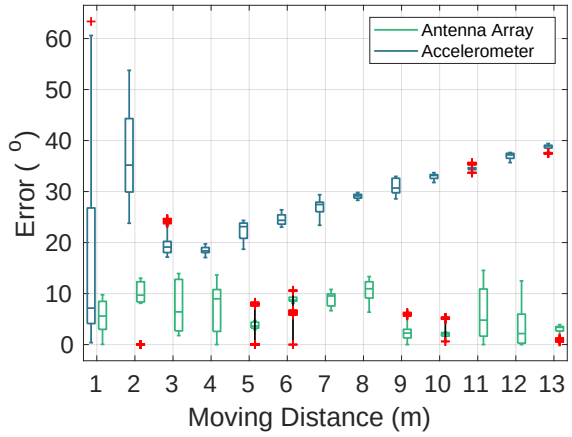


Fig. 14. Drifting Error


[2] W. Kang and Y. Han, "Smartpdr: Smartphone-based pedestrian dead reckoning for indoor localization," *IEEE Sensors journal*, vol. 15, no. 5, pp. 2906–2916, 2014.

[3] C. Wu, Z. Yang, and Y. Liu, "Smartphones based crowdsourcing for indoor localization," *IEEE Transactions on Mobile Computing*, vol. 14, no. 2, pp. 444–457, Feb 2015.

[4] D. Dardari, P. Closas, and P. M. Djurić, "Indoor tracking: Theory, methods, and technologies," *IEEE Transactions on Vehicular Technology*, vol. 64, no. 4, pp. 1263–1278, April 2015.

[5] Z. Ren, J. Yuan, J. Meng, and Z. Zhang, "Robust part-based hand gesture recognition using kinect sensor," *IEEE Transactions on Multimedia*, vol. 15, no. 5, pp. 1110–1120, 2013.

[6] C. Boletsis, "The new era of virtual reality locomotion: a systematic literature review of techniques and a proposed typology," *Multimodal Technologies and Interaction*, vol. 1, no. 4, p. 24, 2017.

[7] "Global indoor positioning and indoor navigation (ipin) market," https://www.technavio.com/report/global-machine-machine-m2m-and-connected-devices-global-indoor-positioning-and-indoor.

[8] S. Lee, B. Kim, H. Kim, R. Ha, and H. Cha, "Inertial sensor-based indoor pedestrian localization with minimum 802.15.4a configuration," *IEEE Transactions on Industrial Informatics*, vol. 7, no. 3, pp. 455–466, 2011.

[9] F. Li, C. Zhao, G. Ding, J. Gong, C. Liu, and F. Zhao, "A reliable and accurate indoor localization method using phone inertial sensors," in *Proceedings of the 2012 ACM conference on ubiquitous computing*. ACM, 2012, pp. 421–430.

[10] N. Roy, H. Wang, and R. Roy Choudhury, "I am a smartphone and i can tell my user's walking direction," in *Proceedings of the 12th annual international conference on Mobile systems, applications, and services*. ACM, 2014, pp. 329–342.

[11] W. Kang, S. Nam, Y. Han, and S. Lee, "Improved heading estimation for smartphone-based indoor positioning systems." in *PIMRC*, 2012, pp. 2449–2453.

[12] N. Mohssen, R. Momtaz, H. Aly, and M. Youssef, "It's the human that matters: Accurate user orientation estimation for mobile computing applications," in *Proceedings of the 11th International Conference on Mobile and Ubiquitous Systems: Computing, Networking and Services*, ser. MOBIQUITOUS '14, 2014, p. 70–79.

[13] P. Zhou, M. Li, and G. Shen, "Use it free: Instantly knowing your phone attitude," in *Proceedings of the 20th annual international conference on Mobile computing and networking*. ACM, 2014, pp. 605–616.

[14] S. Shen, M. Gowda, and R. Roy Choudhury, "Closing the gaps in inertial motion tracking," in *Proceedings of the 24th Annual International Conference on Mobile Computing and Networking*. ACM, 2018, pp. 429–444.

[15] B. Wang, Q. Xu, C. Chen, F. Zhang, and K. J. R. Liu, "The promise of radio analytics: A future paradigm of wireless positioning, tracking, and sensing," *IEEE Signal Processing Magazine*, vol. 35, no. 3, pp. 59–80, May 2018.

[16] K. R. Liu and B. Wang, *Wireless AI: Wireless Sensing, Positioning, IoT, and Communications*. Cambridge University Press, 2019.

[17] M. Kotaru, K. Joshi, D. Bharadia, and S. Katti, "Spotfi: Decimeter level localization using wifi," in *ACM SIGCOMM computer communication review*, vol. 45, no. 4. ACM, 2015, pp. 269–282.

[18] J. Xiong and K. Jamieson, "Arraytrack: A fine-grained indoor location system," in *Presented as part of the 10th USENIX Symposium on Networked Systems Design and Implementation (NSDI 13)*. Lombard, IL: USENIX, 2013, pp. 71–84.

[19] C. Wu, F. Zhang, Y. Fan, and K. J. R. Liu, "Rf-based inertial measurement," in *Proceedings of the ACM Special Interest Group on Data Communication*, ser. SIGCOMM '19. New York, NY, USA: ACM, 2019, pp. 117–129.

[20] Y. Fan, F. Zhang, C. Wu, B. Wang, and K. J. R. Liu, "Indoor heading direction estimation using rf signals," in *ICASSP 2020 - 2020 IEEE International Conference on Acoustics, Speech and Signal Processing (ICASSP)*, 2020, pp. 1628–1632.

[21] F. Zhang, C. Chen, B. Wang, H. Lai, Y. Han, and K. J. R. Liu, "Wiball: A time-reversal focusing ball method for decimeter-accuracy indoor tracking," *IEEE Internet of Things Journal*, vol. 5, no. 5, pp. 4031–4041, Oct 2018.

[22] S. Ayub, B. M. Heravi, A. Bahraminasab, and B. Honary, "Pedestrian direction of movement determination using smartphone," in *2012 Sixth International Conference on Next Generation Mobile Applications, Services and Technologies*, 2012, pp. 64–69.

[23] S. Kumar, S. Gil, D. Katabi, and D. Rus, "Accurate indoor localization with zero start-up cost," in *Proceedings of the 20th annual international conference on Mobile computing and networking*. ACM, 2014, pp. 483–494.

[24] W. Gong and J. Liu, "Sifi: Pushing the limit of time-based wifi localization using a single commodity access point," *Proceedings of the ACM on Interactive, Mobile, Wearable and Ubiquitous Technologies*, vol. 2, no. 1, pp. 1–21, 2018.

[25] S. Sen, J. Lee, K.-H. Kim, and P. Congdon, "Avoiding multipath to revive inbuilding wifi localization," in *Proceeding of the 11th annual international conference on Mobile systems, applications, and services*. ACM, 2013, pp. 249–262.

[26] Y. Xie, J. Xiong, M. Li, and K. Jamieson, "md-track: Leveraging multi-dimensionality for passive indoor wi-fi tracking," in *The 25th Annual International Conference on Mobile Computing and Networking*, 2019, pp. 1–16.

[27] K. Qian, C. Wu, Y. Zhang, G. Zhang, Z. Yang, and Y. Liu, "Widar2. 0: Passive human tracking with a single wi-fi link," in *Proceedings of the 16th Annual International Conference on Mobile Systems, Applications, and Services*. ACM, 2018, pp. 350–361.

[28] D. Vasisht, S. Kumar, and D. Katabi, "Decimeter-level localization with a single wifi access point," in *13th {USENIX} Symposium on Networked Systems Design and Implementation ({NSDI} 16)*, 2016, pp. 165–178.

[29] Y. Xie, Z. Li, and M. Li, "Precise power delay profiling with commodity wi-fi," *IEEE Transactions on Mobile Computing*, vol. 18, no. 6, pp. 1342–1355, 2018.

[30] M. Youssef and A. Agrawala, "The horus wlan location determination system," in *Proceedings of the 3rd International Conference on Mobile Systems, Applications, and Services*, ser. MobiSys '05. New York, NY, USA: ACM, 2005, pp. 205–218.

[31] X. Wang, L. Gao, and S. Mao, "Phasefi: Phase fingerprinting for indoor localization with a deep learning approach," in *2015 IEEE Global Communications Conference (GLOBECOM)*, 2015, pp. 1–6.

[32] P. Bahl and V. N. Padmanabhan, "Radar: an in-building rf-based user location and tracking system," in *Proceedings IEEE INFOCOM 2000. Conference on Computer Communications. Nineteenth Annual Joint Conference of the IEEE Computer and Communications Societies (Cat. No.00CH37064)*, vol. 2, March 2000, pp. 775–784 vol.2.

[33] Z. Wu, Y. Han, Y. Chen, and K. J. R. Liu, "A time-reversal paradigm for indoor positioning system," *IEEE Transactions on Vehicular Technology*, vol. 64, no. 4, pp. 1331–1339, April 2015.

[34] C. Chen, Y. Chen, Y. Han, H. Lai, F. Zhang, and K. J. R. Liu, "Achieving centimeter-accuracy indoor localization on wifi platforms: A multi-antenna approach," *IEEE Internet of Things Journal*, vol. 4, no. 1, pp. 122–134, Feb 2017.

[35] C. Chen, Y. Chen, Y. Han, H. Lai, and K. J. R. Liu, "Achieving centimeter-accuracy indoor localization on wifi platforms: A frequency hopping approach," *IEEE Internet of Things Journal*, vol. 4, no. 1, pp. 111–121, Feb 2017.

[36] D. Wu, D. Zhang, C. Xu, Y. Wang, and H. Wang, "Widir: Walking direction estimation using wireless signals," in *Proceedings of the 2016 ACM International Joint Conference on Pervasive and Ubiquitous Computing*, ser. UbiComp '16. New York, NY, USA: ACM, 2016, pp. 351–362.

[37] G. Lerosey, J. De Rosny, A. Tourin, A. Derode, G. Montaldo, and M. Fink, "Time reversal of electromagnetic waves," *Physical review letters*, vol. 92, no. 19, p. 193904, 2004.